Journal of Ultrafine Grained and Nanostructured Materials
https://jufgnsm.ut.ac.ir
Vol. 56, No.1, June 2023, pp. 108-120
Print ISSN: 2423-6845 Online ISSN: 2423-6837
DOI: 10.22059/jufgnsm.2023.01.11

Structural, Electrical and Optical Characterization of ZnO:Li Thin Films Prepared by Sol-Gel Spin Coating

P. Khosravi, S. A. Seyyed Ebrahimi*

Advanced Magnetic Materials Research Center, School of Metallurgy and Materials, College of Engineering, University of Tehran, Tehran, Iran.

Recieved: 9 May 2023; Accepted: 25 June 2023

**Corresponding author email: saseyyed@ut.ac.ir*

ABSTRACT

Li-doped ZnO thin films prepared by sol-gel spin coating method, have been studied in this research to increase the p-type ZnO layers conduc-tivity. For this purpose, the lithium dopant concentration was changed and structural, electrical, and optical properties of the layers were in-vestigated. Structural investigations showed that the single phase layers with wurtzite hexagonal structure and 40-50 nm average grain size were formed. For obtaining p-type layers and enhancing their electrical conductivity, there was an optimum in moderate doping concentra-tions (in 0.4 Li/Zn ratio in sol). Furthermore, regarding the optical properties, it was concluded that the band gap energy is sensitive to Li con-centration and changes from 3.27 eV in pure layer to 3.16 eV in heavy Li doped layer. Besides, the refractive index of ZnO layer decreased with Li doping. This can be due to moth eye effect. Finally, a novel mechanism was developed by DFT which is in accordance with electrical and optical observations. These calculations propose the activation of a self-compensation mechanism by Li doping which can be responsible for the decrease of the conductivity at high Li concentrations. In the proposed mechanism, Zni donor defect sites, accompanying LiZn sites, cause self-compensation.

Keywords: *ZnO; Thin-film; Sol-gel; Optoelectronics; Li-doping*

1. Introduction

Zinc oxide, with direct optical band gap of 3.25 eV at room temperature and high exciton energy (60 meV at room temperature), is a good choice for using in electronics and optoelectronics applications [1-3] including photodetectors [4, 5], thin film transistors [6, 7], piezoelectric nano generators [8, 9], gas-sensors [10, 11], bio-sensors [12], and particularly UV-blue light emitting devices [13].

Zinc oxide (ZnO) optoelectronic applications were considered since the first GaN (Gallium Nitride)/ InGaN based Light Emitting Diode (LED) was made in 90s. ZnO has approximately same band gap as GaN but with more benefits including higher exciton energy (60 meV vs. 24 meV for GaN), possibility of band gap engineering (from 3 to 4.5 eV), possibility of coating on different substrates, lower annealing temperature (500 °C vs. more than 1000 °C

for GaN), easy processing, higher resistance to radiation, lower cost, and non-toxicity [14].

Usually undoped ZnO shows n-type conductivity. The native defects like vacancy of oxygen (V_O) and interstitial zinc (Zn_i) are mostly known responsible for this phenomenon; besides, the site which a dopant occupies in lattice is important and by its changing an acceptor dopant can become a donor [1]. For these reasons, making p-type ZnO is challenging.

The full potential of ZnO as a semiconductor cannot be achieved before preparing stable p-type with suitable conductivity due to low effectiveness of p-n junction and bipolar devices [15]. The researches on this field is still ongoing [15, 16]. Different elements from group V and I have been used as acceptor dopant by either mono-doping or co-doping [1, 17]. According to these researches, group V elements except N, tend to form A_{Zn}-$2V_{Zn}$ (A= P, As, Sb) complexes rather than sitting in O sites and form shallow acceptor levels. Element N also makes N_O-V_{Zn} complexes for providing shallow acceptor levels. However, these complexes are highly sensitive to growth and post-growth treatments. For this reason, a part of researches focused on co-doping techniques. But co-doping has some disadvantages too, including more defects formation which cause more scattering. This makes necessarily using expensive and complicated methods like MBE, which are more powerful in producing low defect layers. Besides, the study and design of these layers are too complicated. Therefore, co-doped layers have still problem in achieving stable p-type [17].

Group I elements are another choice, particularly for their shallower acceptor levels rather than group V elements. Among them, Li have theoretically the shallowest acceptor level [1, 18-20]. However, group I elements, have its own challenges due to their action as donor in interstitial sites[14].

According to the above discussions, lithium from group I, showing shallowest acceptor levels during substitution in Zn site (Li_{Zn}), was selected in this research as a p-type dopant while only few theoretical works has been reported on it so far [18, 19].

Li p-type doping is difficult because of self-compensation effects. This effect will be happened due to either Li in interstitial sites (Li_i) or intrinsic donor defects, including Zinc anti-site (Zn_O), Oxygen vacancy (V_O) and Zinc interstitial (Zn_i). However, among these defects, the Zn_O defect has a high formation energy and does not expected to be presented significantly in the lattice [1]. As a result of self-compensation, despite two decades of theoretical and experimental works on Li doping, this doping system, like other acceptor doping systems, still have been unable to yield an effective conductive p-type ZnO widely applicable in optoelectronics and this field is still an open issue [21, 22].

For preparation of ZnO thin film, diverse methods have been used. Sputtering [23-25], CVD [26, 27], and PLD [28-30] are more convenient especially for coating p-type layers. Wet chemical methods including sol-gel [31, 32], spray pyrolysis [33, 34], and co-precipitation [35, 36] are also used for synthesis of ZnO nanostructures; however, they are less convenient for p-type layers.

In this work, we used sol-gel spin coating which is a very simple and low-cost method for preparing ZnO thin films. The major goal of this work was to obtain the conductive p-type ZnO layer by optimizing the lithium doping. Furthermore, the investigation of optical properties is necessary for the recognition of the layers' performance in optoelectronic applications. For further study of the proposed mechanism for the electrical and optical properties, Li-doped ZnO structures were studied by DFT calculations. According to our knowledge, the mechanism for self-compensation proposed in this work was not reported elsewhere.

Therefore, using a simple method for the production of Li-doped p-type layer with acceptable conductivity as well as proposing a novel mechanism for the self-compensation effect are the major differences between this work and the others.

2. Experimental procedure

8 g Zinc acetate dehydrate (ZAD, Fluka, ≥ 99.0%) as precursor, 8 ml monoethanol amine (MEA, Merck, ≥ 99.5%) as sol stabilizer, 92 ml ethanol (Merck,≥ 99.9%) as solvent were mixed for preparing 100 ml of 0.35 M sol with MEA/ZAD molar ratio of 4. Lithium nitride (Merck, 99.995%) was also used in different concentrations as precursor for Li doping.

The above contents were stirred for 1 hr at 60-70 °C with speed of 140-180 rpm by a hot plate using a reflux system until a yellowish transparent sol appeared. This sol aged for 1 day before being used.

For preparing thin film, sol were dropped onto glass or silicon substrates (silicon substrates were used for only electrical properties tests). Then substrate was spun for 30 s with 3000 rpm speed by spin coater. After each spin coating stage, for layer stabilization, the specimen pre-annealed at 350 °C for 6 min. This cycle was repeated four times. Finally, the layer annealed in a tube furnace for 1 hr at 500 °C.

The samples were characterized by X-Ray Diffraction (Philips X-Ray Diffractometer using the Cu Kα radiations, located in School of Metallurgy and Materials, University of Tehran) and Field Emission Scanning Electron Microscope (HITACHI S4160, located in School of Electrical and Computer Engineering, University of Tehran) and the average grain size, average particle size, preferential direction and surface topography were studied. The electrical parameters including type of majority carriers and conductivity were measured by four point probe surface resistance measurement tool equipped with rectifying method extension (Sherescan, located in School of Electrical and Computer Engineering, University of Tehran). The rectifying method extension is used for determining semiconductor type. In this method, three of four probes are used. Between first and second probes, an AC current is injected and the resulting DC component of voltage, between second and third probes, is measured. The semiconductor type is determined by the polarity of DC component based on rectifying properties of metal-semiconductor contact. Finally, the optical properties were investigated by transmission Ultra Violet-Visible spectroscopy (equipment located in Nanoscience and Technology Research Center, University of Tehran) and reflection Ultra Violet-Visible spectroscopy (equipment located in Institute for Nanoscience and Nanotechnology, Sharif University of Technology) and photoluminescence spectroscopy (equipment located in Nanoscience and Technology Research Center, University of Tehran). Optical band gap and Urbach energy were calculated from the optical results.

For evaluating the proposed mechanism for some observations, Density Function Theory (DFT) calculations and analyses were used. For more details see Supplementary.

3. Results and discussion

The layers coated on glass substrate with different Li/Zn atomic ratios in sol (0, 0.2, 0.4, and 0.6) were prepared. It should be considered that there is different amount of Li in films. Li/Zn ratio in layers is one order of magnitude lower than this ratio in sol (See Supplementary).

The layers were investigated by XRD, as shown in Fig. 1 which indicates Wurtzite hexagonal structure (Reference code: 00-001-1136) for all of the films; besides, it can be conclud-

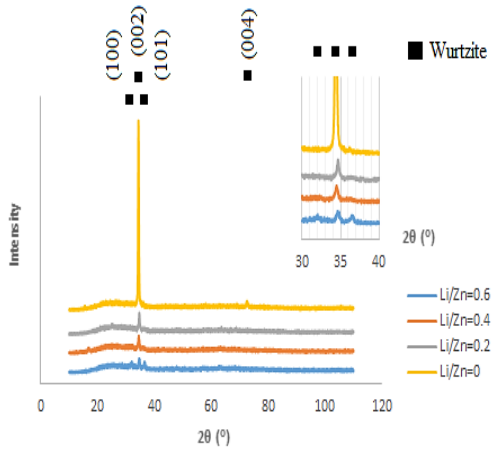

Fig. 1- XRD spectra of the layers with different Li/Zn atomic ratios in sol.

ed that all of the thin films are highly (002) (c-axis) oriented. The preferential orientation decreased by increasing Li content. This can be due to using lithium nitride which burns during annealing and destructs the structure.

The grain size of the specimens have been calculated by Scherrer equation, as shown in table 1. It can be seen that the grain size variation is negligible.

FESEM images of two samples with Li/Zn ratio of 0 and 0.4 are shown in Fig. 2. As can be seen, the surface of Li free specimen is smooth but the doped one has a rough surface. It can be seen that a wrinkle network has been formed on the surface of layer by Li-doping. This phenomenon was previously reported by doping of another IA group element, Na [37]. Fig. 3 shows the cross section of the layer with Li/Zn atomic ratio of 0.4. The thickness of this layer is determined 260 nm.

The electrical conductivity and type were characterized for the different layers which are shown in table 1. The pure ZnO is n-type because of the presence of defects like V_O and Zn_i; however, by increasing lithium the effect of these defects were compensated and finally the samples with more than 0.3 Li/Zn atomic ratio became p-type and the layer with 0.4 Li/Zn atomic ratio is the most conductive one. The 0.4 Li/Zn ratio specimen's conductivity and type measured for 30 days. This specimen showed stable electrical properties during this period.

In p-type samples, by increasing lithium percentage, firstly there is an increase in conductivity and then it changes into a decrease. The reason of the former can be the increasing of holes density by increasing Li acceptor dop-

Table 1- The average grain size, resistance and majorities' carrier type of the layers with different Li/Zn atomic ratio in sol

Li/Zn	Average grain size (nm)	Resistance (μΩ.cm)	Type
0	47	549	n
0.2	44	575	i
0.3	-	572	p
0.4	42	551	p
0.6	47	572	p

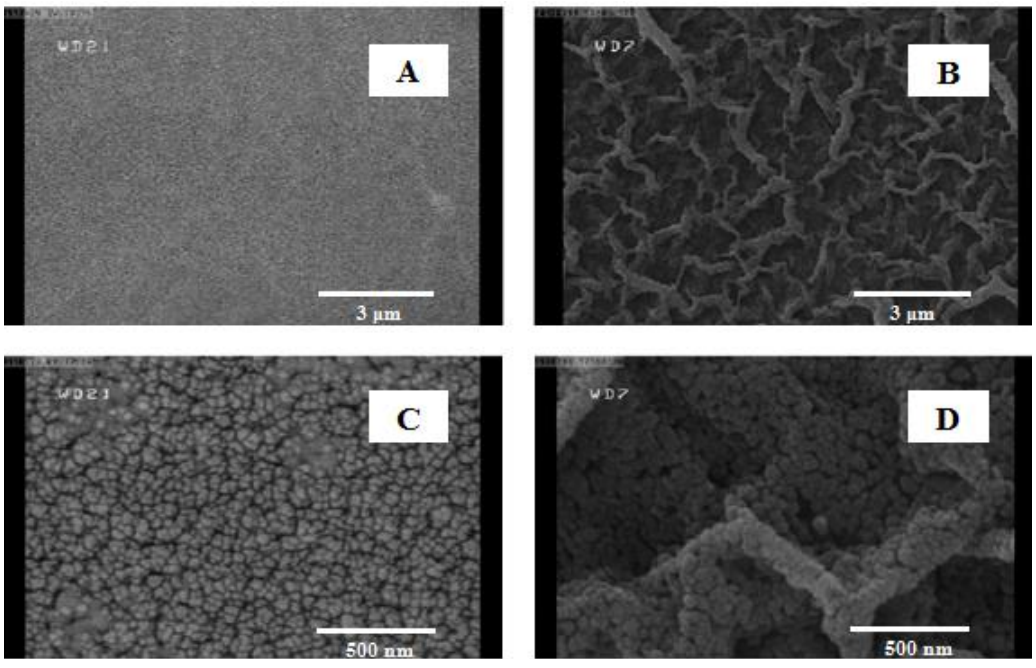

Fig. 2- FESEM images from the surface of the samples with Li/Zn ratios of a,c) 0 and b,d) 0.4.

ants density. On the other hand, in heavier doping, the distortion of lattice can be responsible for the decrease of conductivity. In fact by adding Li into lattice, especially by using a nitride precursor, increase of defects and lattice distortion is expected which is in accordance with XRD results as well. Besides, from another point of view, according to DFT calculations (see supplementary), it was proved that Li effects on defects' formation energy. It has been specifically shown by these calculations that the presence of Li, decreases the Zn_i formation energy which is a donor. Therefore, another possible mechanism for decreasing resistivity can be increasing of donor defects' concentration because of lowered formation energies in presence of acceptor Li dopant. This phenomenon is called self-compensation. Especially in higher concentrations, it is expected that this effect strengthened because there are not enough V_{Zn} sites in the lattice to be occupied by Li.

Fig. 4 shows the UV-Visible spectroscopy results of the specimens and uncoated glass substrate (Fig. 4). By comparison of uncoated glass spectrum and other specimens' spectra, it can be concluded that the first sharp increase in transmittance of the samples is the substrate effect.

The average transmittance of visible light (400-700 nm) for these layers are shown in Fig. 5. By increasing the lithium content, the transmittance decreased, which can be attributed to the scattering of light created by increasing lattice defects due to increasing doping [38]. Besides, the more rapid decrease of transmittance from 0.4 Li/Zn ratio (p-type samples) could be also assigned to the light absorption by the holes.

The bandgaps of the samples are determined from the UV-Visible results by Tauc method [39, 40]. The Tauc plots are shown in Fig. 4 and the measured values are shown in Fig. 6. The layer with 0.2 Li/ Zn ratio has a lower bandgap than 0 and 0.4 ratios. This can be due to the lack of Burstein-Moss effect in this specimen which is intrinsic [39]. Besides, there is a decreasing trend for bandgap in p-type layers which is consistent with band gap narrowing (BGN) effect happens by heavy doping in which the acceptor states degenerate and con-

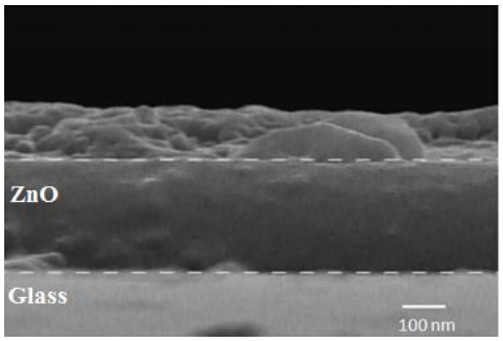

Fig. 3- FESEM cross section of the layer with 0.4 Li/Zn atomic ratio.

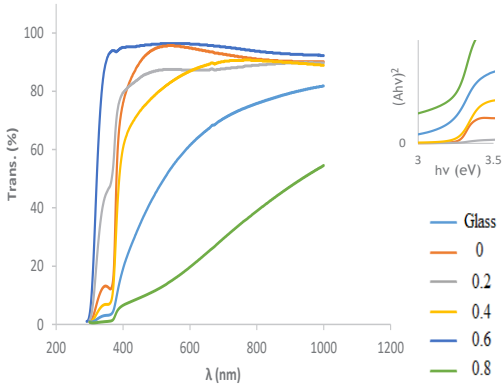

Fig. 4- The UV-Visible spectroscopy of the layers with different atomic Li/Zn ratios and substrate. The Tauc plots of the specimens are shown in the inset (top right).

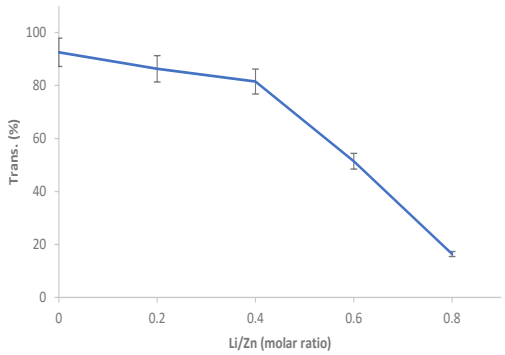

Fig. 5- The average transmittance vs. Li/Zn atomic ratio in sol.

sequently the new band joins to the valance band and reduce the bandgap [41].

From the UV-Visible results, Urbach energy of the samples could also be obtained [40] which are shown with bandgaps in table 2 (for Urbach plots see Fig. S11 in Supplementary).

The increase of Urbach energy with the increasing of dopants in p-type samples shows the increase of local states and subsequently increase of the defects, which confirms the decreasing transmittance (Fig. 5) previously attributed to. Besides, it is in accordance with XRD analyses which shows destruction in crystal quality by doping. As discussed previously, in accordance with these results, DFT predicts a self-compensation mechanism which can facilitate formation of some defects, especially at high concentrations.

The pure ZnO layer and the layer with the best electrical conductivity (0.4 ratio) were characterized by photoluminescence spectroscopy. The results are shown in Fig. 7 which demonstrates a broad peak which represents band gap and near band emissions related to the defects including Zn_i and Li_{Zn} [1]. PL emission have more intensities for the doped layer which can be due to highest defects in doped layer which is consistent with the increase of Urbach energy. Two of the most expected defects after doping are Li_{Zn} and Zn_i. The formation energies for Li_{Zn} and Zn_i have been calculated by DFT (see supplementary). The formation energies for Zn_i and Li_{Zn} are 3.2 and 1.8 eV respectively; however, the formation energy of the both in the lattice is 0.9 eV. Therefore, the presence of Li_{Zn} acceptor sites make Zn_i donor defects more preferable. This cause a self-compensation effect which have destructive impact on the efficiency of acceptor dopant and lowers the electrical conductivity, and can explain some of the optical and electrical behaviors discussed before.

In addition to the transmission UV-Visible spectroscopy, these layers (0 and 0.4 Li/Zn ratio) were examined by the reflection UV-Visible spectroscopy. The n-λ (refractive index vs. light wavelength) plots of this test are shown in Fig. 8. The figure shows that the refractive index decreased by adding lithium to the lattice. This can be due to the increasing surface

Table 2- The band gap and Urbach energy of the layers with different Li/Zn atomic ratios in sol.

Li/Zn	Band gap (eV)	Urbach energy (meV)
0	3.27	76
0.2	3.25	150
0.4	3.26	126
0.6	3.17	510
0.8	3.16	914

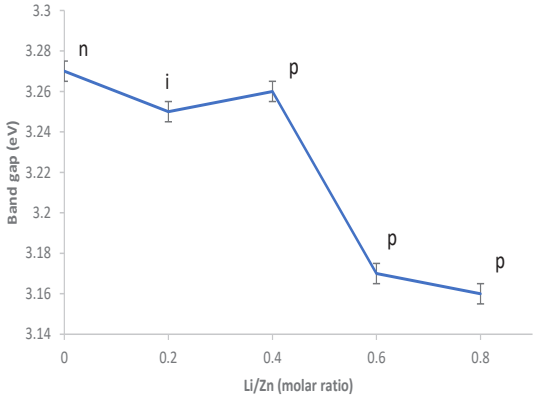

Fig. 6- Band gap vs. Li/Zn atomic ratio in sol.

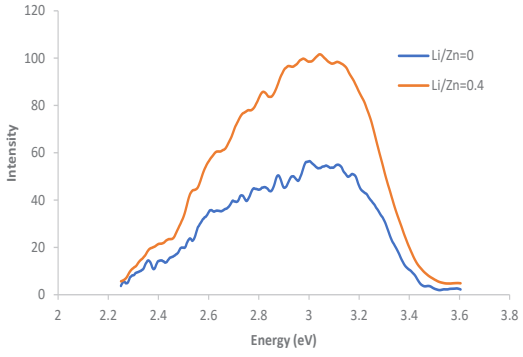

Fig. 7- The PL spectra of layers with 0 and 0.4 Li/Zn atomic ratios.

roughness, according to moth eye effect [42, 43], which is consistent with Fig. 2b. The moth eye effect happens when the surface have lateral dimension smaller than the light's wavelength. This type of surface reduce the reflection due to making a refractive index gradient between air and thin film (see Fig. 9) [42, 43]. This low refractive index could also be desirable in many optoelectronics applications while usually the semiconductors have a large refractive index which causes a high waste of light.

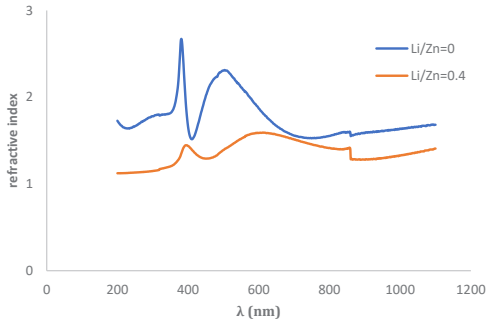

Fig. 8- The average transmittance vs. Li/Zn atomic ratio in sol.

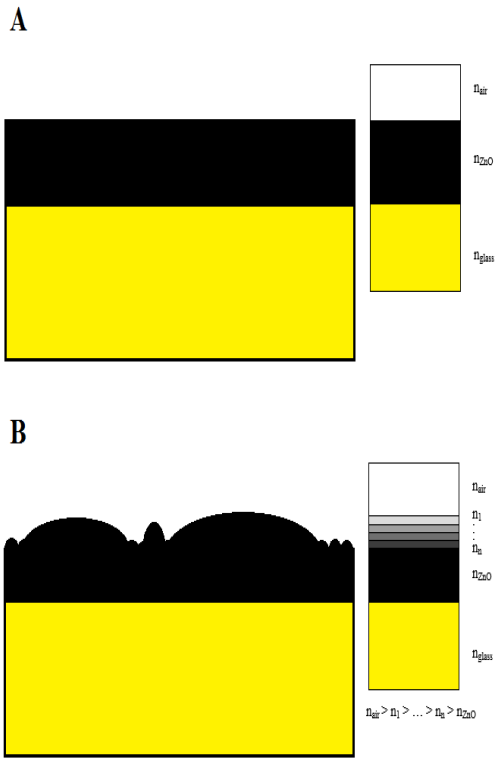

Fig. 9- The comparison between refractive index of a smooth surface and a surface with submicronic bumps.

4. Conclusions

In this research, Li-doped ZnO thin films were prepared by sol-gel spin coating method. All of the layers had Wurtzite hexagonal structure with 40-50 nm average grain size and c-axis preferential direction. The Li-doping made the layers p-type successfully. The best conductivity of p-type layers was achieved in a moderate Li concentration. The investigations show that the p-type layer is stable for at least 30 days. The results also showed the sensitivity of ZnO layer band gap to Li concentration which makes Li a candidate for band gap engineering. Besides, Li doping caused a decrease in refractive index. This could be due to moth eye effect because the doping made the layer's surface uneven. The lower refractive index is desirable in optoelectronics applications. The PL emission's intensity increases by Li doping which can be desired in optoelectronic applications. By DFT calculations, a self-compensation effect by Zn_i defects has been predicted which can be the responsible mechanism for the decrease of conductivity in high Li doping and the increase of PL emissions intensity in Li-doped layer.

References

1. P. Capper, S. Kasap, and A. Willoughby, Zinc oxide materials for electronic and optoelectronic device applications: John Wiley & Sons, 2011.

2. T. Makino, Y. Segawa, M. Kawasaki, A. Ohtomo, R. Shiroki, K. Tamura, et al., "Band gap engineering based on Mg x Zn 1– x O and Cd y Zn 1– y O ternary alloy films," Applied Physics Letters, vol. 78, pp. 1237-1239, 2001.

3. A. Venkatanarayanan and E. Spain, "Review of recent developments in sensing materials," 2014.

4. L. Mandalapu, Z. Yang, F. Xiu, D. Zhao, and J. Liu, "Homojunction photodiodes based on Sb-doped p-type ZnO for ultraviolet detection," Applied physics letters, vol. 88, p. 092103, 2006.

5. W. Ouyang, J. Chen, Z. Shi, and X. Fang, "Self-powered UV photodetectors based on ZnO nanomaterials," Applied Physics Reviews, vol. 8, p. 031315, 2021.

6. R. Hoffman, B. J. Norris, and J. Wager, "ZnO-based transparent thin-film transistors," Applied Physics Letters, vol. 82, pp. 733-735, 2003.

7. D. Zhu, Z. Jiang, W. Zhang, D. Yin, W. Xu, S. Han, et al., "Room-temperature fabrication of high-performance H doped ZnO thin-film transistors," Materials Chemistry and Physics, vol. 261, p. 124248, 2021.

8. S. Hazra and S. Basu, "Hydrogen sensitivity of ZnO p–n homojunctions," Sensors and Actuators B: Chemical, vol. 117, pp. 177-182, 2006.

9. A. T. Le, M. Ahmadipour, and S.-Y. Pung, "A review on ZnO-based piezoelectric nanogenerators: Synthesis, characterization techniques, performance enhancement and applications," Journal of Alloys and Compounds, vol. 844, p. 156172, 2020.

10. S. Pati, A. Maity, P. Banerji, and S. Majumder, "Qualitative and quantitative differentiation of gases using ZnO thin film gas sensors and pattern recognition analysis," Analyst, vol. 139, pp. 1796-1800, 2014.

11. M. A. Franco, P. P. Conti, R. S. Andre, and D. S. Correa, "A review on chemiresistive ZnO gas sensors," Sensors and Actuators Reports, p. 100100, 2022.

12. C. Xu, C. Yang, B. Gu, and S. Fang, "Nanostructured ZnO for biosensing applications," Chinese Science Bulletin, vol. 58, pp. 2563-2566, 2013.

13. J. H. Lim, C. K. Kang, K. K. Kim, I. K. Park, D. K. Hwang, and S. J. Park, "UV electroluminescence emission from ZnO light-emitting diodes grown by high-temperature radiofrequency sputtering," Advanced Materials, vol. 18, pp. 2720-2724, 2006.

14. J. C. Fan, K. Sreekanth, Z. Xie, S. Chang, and K. V. Rao, "p-Type ZnO materials: theory, growth, properties and devices," Progress in Materials Science, vol. 58, pp. 874-985, 2013.

15. C.-Y. Tsay and W.-Y. Chiu, "Enhanced electrical properties and stability of p-type conduction in zno transparent semiconductor thin films by co-doping ga and n," Coatings, vol. 10, p. 1069, 2020.

16. S. Guan, T. Zhan, L. Hao, S. Kurosu, T. Ukai, X. Zhao, et al., "Understanding the role of potassium incorporation in realizing transparent p-type ZnO thin films," Journal of Alloys and Compounds, vol. 904, p. 164070, 2022.

17. Z. Ye, H. He, and L. Jiang, "Co-doping: an effective strategy for achieving stable p-type ZnO thin films," Nano Energy, vol. 52, pp. 527-540, 2018.

18. T. Yamamoto and H. Katayama-Yoshida, "Unipolarity of ZnO with a wide-band gap and its solution using codoping method," Journal of crystal growth, vol. 214, pp. 552-555, 2000.

19. M. Wardle, J. Goss, and P. Briddon, "Theory of Li in ZnO: A limitation for Li-based p-type doping," Physical Review B, vol. 71, p. 155205, 2005.

20. B. W.-C. Au and K.-Y. Chan, "Sodium and potassium doped P-type ZnO films by sol-gel spin-coating technique," Applied Physics A, vol. 123, p. 485, 2017.

21. Y. Wang, C. Zhou, A. M. Elquist, A. Ghods, V. G. Saravade, N. Lu, et al., "A review of earth abundant ZnO-based materials for thermoelectric and photovoltaic applications," Oxide-based Materials and Devices IX, vol. 10533, pp. 163-179, 2018.

22. N. M. J. Ditshego, "ZnO Nanowire Field-Effect Transistor for Biosensing: A," Nanowires: Recent Progress, p. 3, 2021.

23. R.-C. Chang 1, S.-Y. Chu 1*, K.-Y. Lo 2, S.-C. Lo 2, and Y.-R. Huang 2, "Physical and structural properties of RF magnetron sputtered ZnO films," Integrated Ferroelectrics, vol. 69, pp. 43-53, 2005.

24. G. H. Jo, S.-H. Kim, and J.-H. Koh, "Enhanced electrical and optical properties based on stress reduced graded structure of Al-doped ZnO thin films," Ceramics International, vol. 44, pp. 735-741, 2018.

25. J. Chen, H. Zhang, Q. Chen, F. Husian, and J.-S. Cherng, "Stable p-type nitrogen-doped zinc oxide films prepared by magnetron sputtering," Vacuum, vol. 180, p. 109576, 2020.

26. Z. Lin, C. Zhang, Z. Liang, R. Liu, L. Chi, and P. Wu, "Local Vibration Modes in Phosphorus-Doped ZnO Nanostructure," Integrated Ferroelectrics, vol. 135, pp. 158-164, 2012.

27. Z. Ye, T. Wang, S. Wu, X. Ji, and Q. Zhang, "Na-doped ZnO nanorods fabricated by chemical vapor deposition and their optoelectrical properties," Journal of Alloys and Compounds, vol. 690, pp. 189-194, 2017.

28. W.-S. Noh, J.-A. Lee, J.-H. Lee, Y.-W. Heo, and J.-J. Kim, "Effect of oxygen pressure on the p-type conductivity of Ga, P co-doped ZnO thin film grown by pulsed laser deposition," Ceramics International, vol. 42, pp. 4136-4142, 2016.

29. C. Luo, L.-P. Ho, F. Azad, W. Anwand, M. Butterling, A. Wagner, et al., "Sb-related defects in Sb-doped ZnO thin film grown by pulsed laser deposition," Journal of Applied Physics, vol. 123, p. 161525, 2018.

30. R. Nasser, J.-M. Song, and H. Elhouichet, "Epitaxial growth and properties study of p-type doped ZnO: Sb by PLD," Superlattices and Microstructures, vol. 155, p. 106908, 2021.

31. N. Souza, P. Portes, F. Sato, D. Silva, L. Cótica, I. Santos, et al., "Ferroic behavior induced by oxygen vacancies in Mn-doped ZnO compounds," Integrated Ferroelectrics, vol. 174, pp. 63-70, 2016.

32. W. L. Liu and Y. F. Zhang, "Blueshift of absorption edge and photoluminescence in Al doped ZnO thin films," Integrated Ferroelectrics, vol. 188, pp. 112-120, 2018.

33. A. Hafdallah, A. Azzedine, H. Belhani, M. S. Aida, and N. Attaf, "Effect of the Nozzle-Substrate Distance on the Structural and Optical Properties of ZnO Thin Films Deposited by Spray Pyrolysis Technique," American Journal of Nano Research and Applications, vol. 5, p. 87, 2017.

34. D. Acosta, A. López-Suárez, C. Magaña, and F. Hernández, "Structural, electrical and optical properties of ZnO thin films produced by chemical spray using ethanol in different amounts of the sprayed solution," Thin Solid Films, vol. 653, pp. 309-316, 2018.

35. K. Chongsri and W. Pecharapa, "Structural Properties of Ga-Doped ZnO Nanoparticles Synthesized by Co-Precipitation Process," Integrated Ferroelectrics, vol. 165, pp. 159-166, 2015.

36. R. Noonuruk, W. Mekprasart, T. Supparattanasamai, T. Kanyapan, W. Techitdheera, and W. Pecharapa, "Characterization and phase formation study of ZnO: Sn nanoparticles synthesized by co-precipitation method," Integrated Ferroelectrics, vol. 156, pp. 58-66, 2014.

37. M. A. Basyooni, M. Shaban, and A. M. El Sayed, "Enhanced gas sensing properties of spin-coated Na-doped ZnO nanostructured films," Scientific reports, vol. 7, p. 41716, 2017.

38. S. Shinde, C. Bhosale, and K. Rajpure, "Photoelectrochemical properties of highly mobilized Li-doped ZnO thin films," Journal of Photochemistry and Photobiology B: Biology, vol. 120, pp. 1-9, 2013.

39. G. Xie, L. Fanga, L. Peng, G. Liu, H. Ruan, F. Wu, et al., "Effect of In-doping on the optical constants of ZnO thin films," Physics Procedia, vol. 32, pp. 651-657, 2012.

40. C. Prajapati and P. Sahay, "Influence of In doping on the structural, optical and acetone sensing properties of ZnO nanoparticulate thin films," Materials Science in Semiconductor Processing, vol. 16, pp. 200-210, 2013.

41. U. Lindefelt, "Doping-induced band edge displacements and band gap narrowing in 3C–, 4H–, 6H–SiC, and Si," Journal of Applied Physics, vol. 84, pp. 2628-2637, 1998.s

42. A. Gombert and B. Bläsi, "The moth-eye effect—From fundamentals to commercial exploitation," in Functional properties of bio-inspired surfaces: characterization and technological applications, ed: World Scientific, 2009, pp. 79-102.

43. M. Fox, "Optical properties of solids. Oxford master series in condensed matter physics," Oxf. Univ. Press NY, p. 305, 2001.

supplementary

A) Li/Zn ratio in specimens

Powder specimens were prepared from solutions too. For this purpose, the solution (sol) was stirred under same condition but without reflux. The sol changed into a gel. The gel was annealed in same condition as layers in furnace. The Li containing gel burned with a red flame which is same as Li flame color. The powders' content were examined by Inductively Coupled Plasma (ICP) method. The result is represented in Table S1 and Fig. S1. The ratio of Li/Zn in specimens have a same trend with sols; however, the ratio reduced by one order of magnitude. This can be rooted in the low melting temperature of Li which provides a high vapor pressure during annealing.

B) DFT calcutions

A unit cell of Zn^{2+} and O^{2-} ions with a=b=3.249 , c=5.2042 and α=β=90°, γ=120° was produced by materials studio software. A 2×2×2 (32 atom) superlattice of ZnO was produced subsequently (Fig. S2). In this lattice, Hubbard energies of $U_{p,O}$ = 7 eV and $U_{d,Zn}$ = 12 eV was set. Adding a dopant atom in this lattice makes a Li/Zn ratio of 0.03 which is comparable to this ratio in specimens (Zn_i defect was added with the same ratio to the superlattice.). These lattices were firstly geometrically optimized, then energy states were calculated by CASTEP with GGA-PBE function. In these calculations, 489.8 eV cutoff energy was set. Besides, 4x4x2 and 2x2x1 k-point grids were used for geometry optimization and energy states calculations respectively.

The formation energies of different defects were evaluated by the S1 formula and listed in table S2.

$$E_f = E_2 - E_1 + E_{removed} - E_{added} \quad (S1)$$

In which E_f, E_2, E_1, $E_{removed}$ and E_{added} are respectively formation energy of the specie (defect or dopant), energy of the lattice after adding specie, energy of the lattice before adding specie (pure ZnO), energy of the removed species and the energy of the added species.

These results show that the presence of Li_{Zn} lowers

Table S1- The Li/Zn ratio in specimens prepared by sols with different ratio of Li/Zn

Li/Zn ration in sol	Li/Zn ration in powder
0.2	0.019
0.4	0.045
0.6	0.057

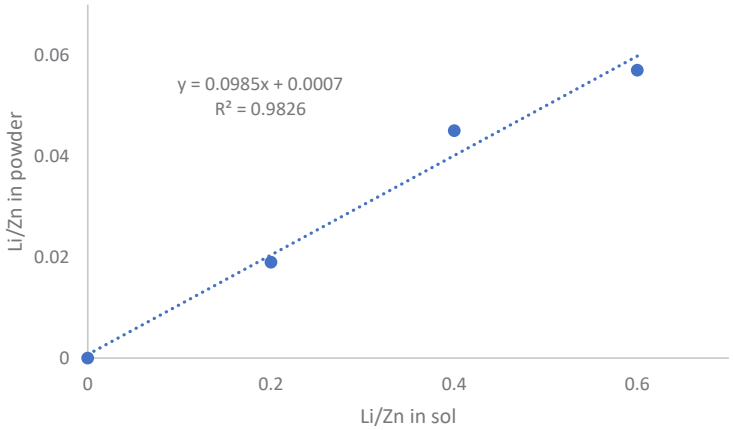

Fig. S1- The Li/Zn ratio in specimens prepared by sols with different ratio of Li/Zn.

the formation energy of Zn_i. This is a self-compensation mechanism which have destructive impact on the efficiency of acceptor dopant and lowers the electrical conductivity.

According to calculations band gap increases by Li doping but decreases by Zn_i (Table S2). It can be seen that the effect of Zn_i is predominant. What studied here was the effect of just two defects on the band gap; however, the real lattice deals with more defects and phenomena.

Besides, Density of state and Band structure diagrams show that Li_{Zn} p orbital makes a state near Valance Band. Therefore, Li in Zn position acts as an acceptor. Zn_i s orbital makes a state near conduction band. In fact a state of ZnO conduction band separates to lower energies. Therefore, Zn_i 's role as a donor is confirmed here (Figs. S3-S10).

Table S2- The formation energy of different species in 2×2×2 lattice

Specie	Formation energy (eV)	E_g (eV)
- (Pure ZnO)	-	3.37
Li_{Zn}	1.8	3.46
Zn_i	3.2	2.74
$Zn_i + Li_{Zn}$	0.9	2.60

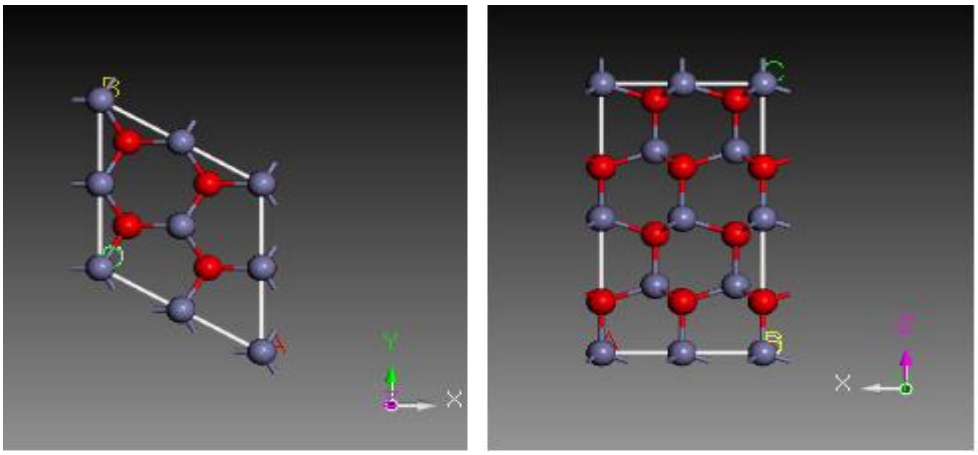

Fig. S2- The Li/Zn ratio in specimens prepared by sols with different ratio of Li/Zn.

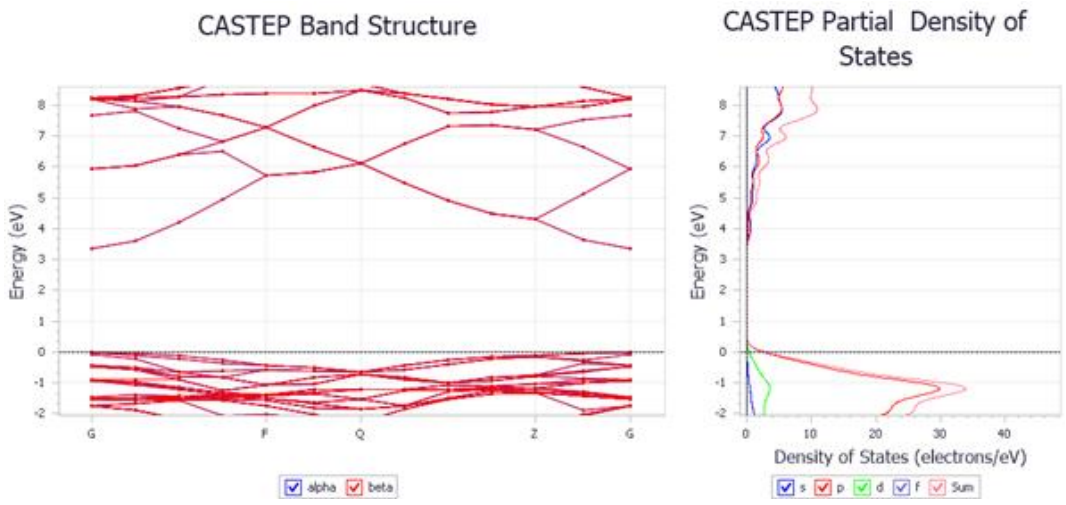

Fig. S3- The Band structure and PDOS diagrams of Pure ZnO.

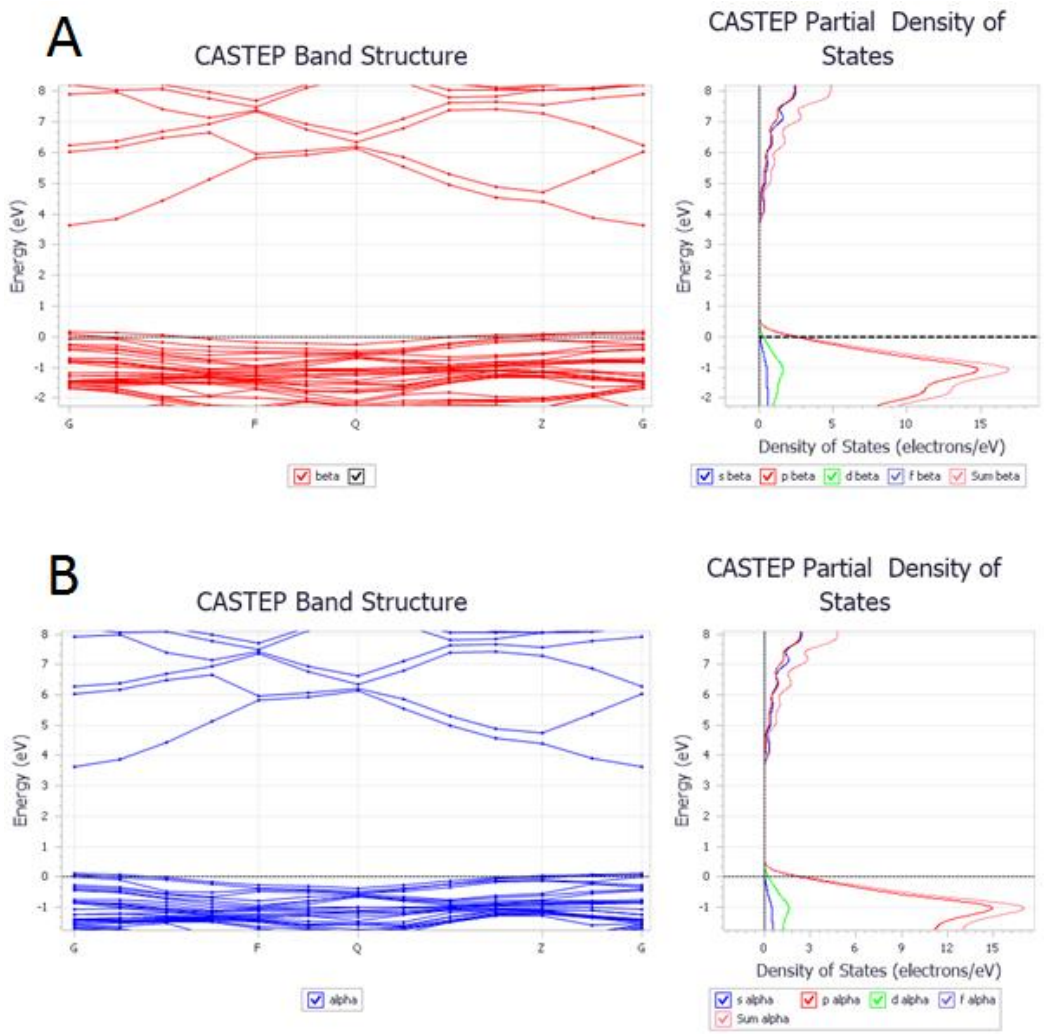

Fig. S4- The spin-down (A) and spin-up (B) Band structure and PDOS diagrams of ZnO:Li_{Zn}.

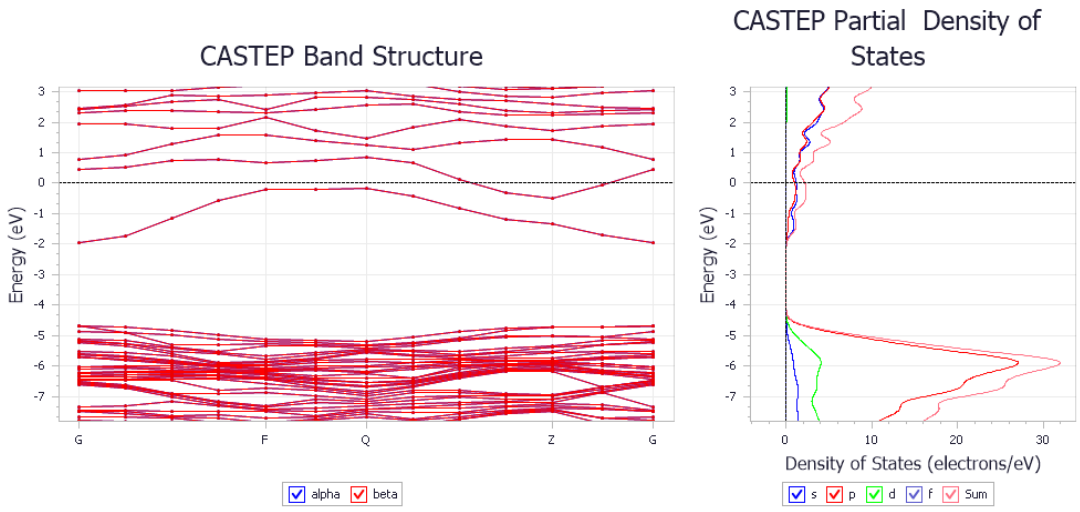

Fig. S5- The Band structure and PDOS diagrams of ZnO:Zn_i.

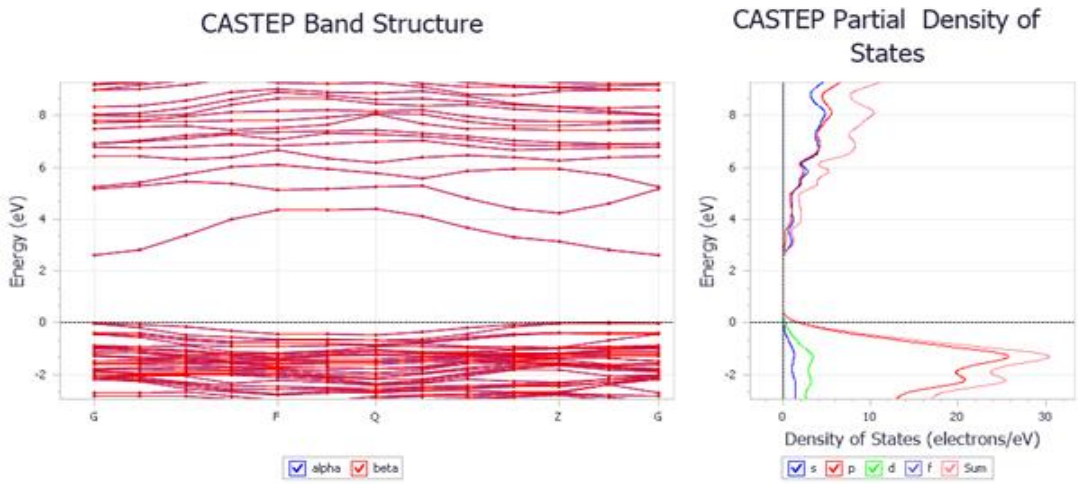

Fig. S6- The Band structure and PDOS diagrams of ZnO:Li_{Zn},Zn_i.

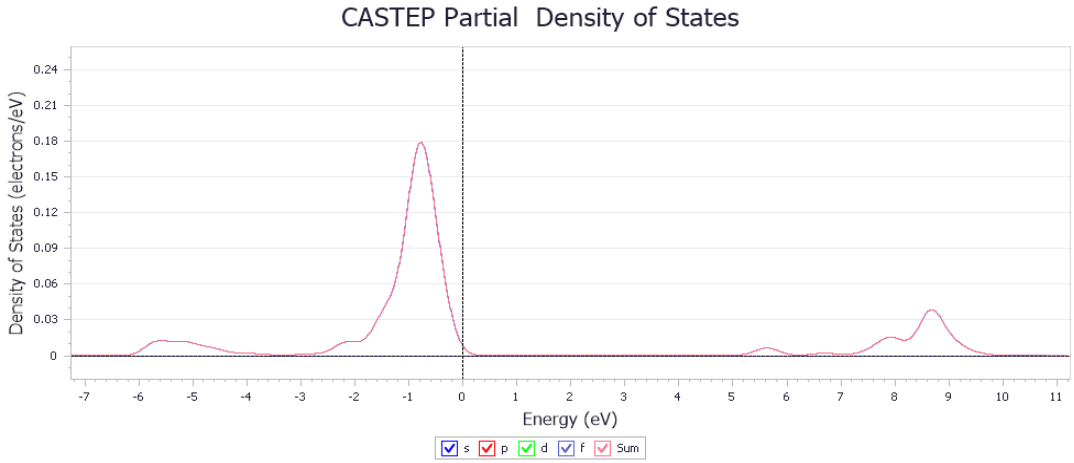

Fig. S7- The PDOS diagrams of Li in ZnO:Li_{Zn}.

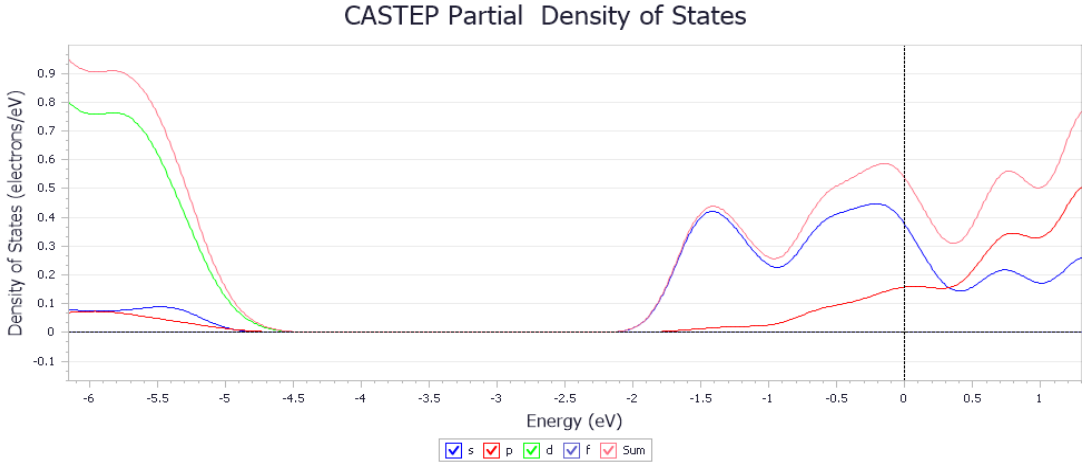

Fig. S8- The PDOS diagrams of Zni in ZnO:Zn_i.

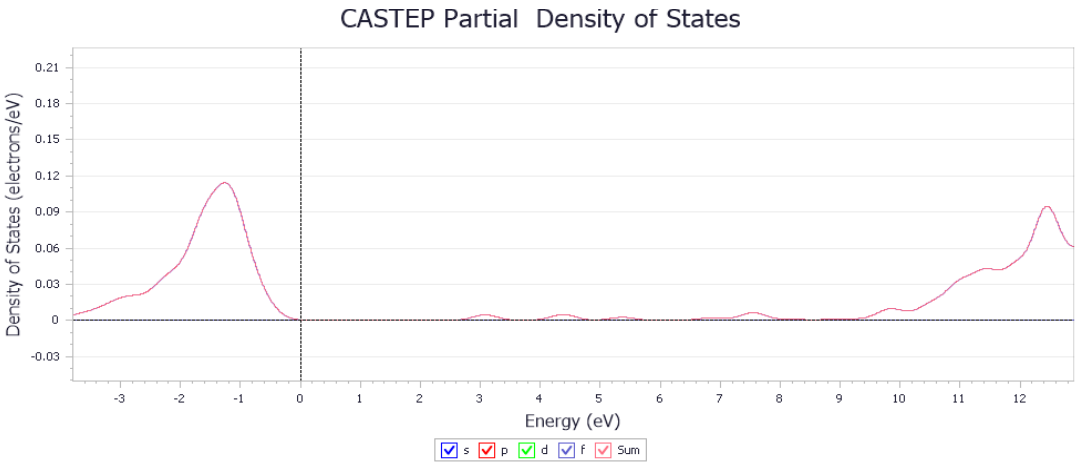

Fig. S8- The PDOS diagrams of Li in ZnO:Li_{Zn}+Zn_i.

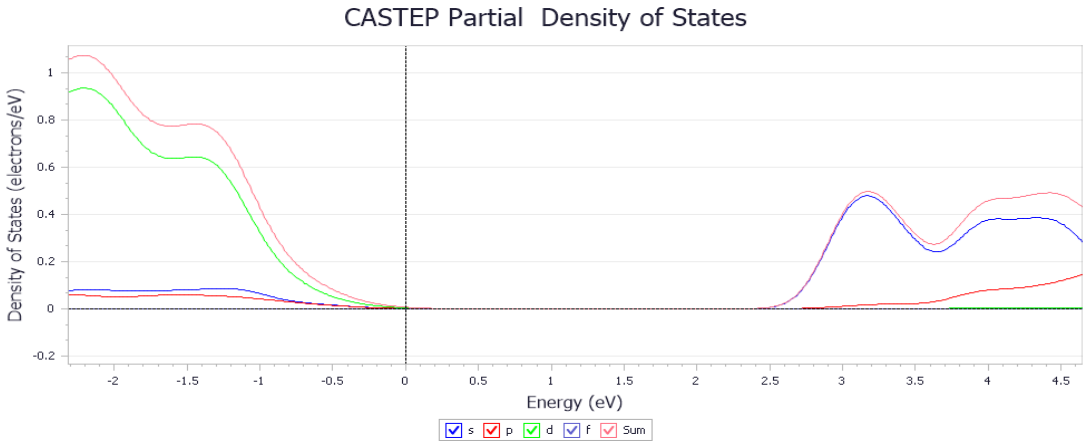

Fig. S9-The PDOS diagrams of Zn_i in ZnO:Li_{Zn}+Zn_i.

C) Urbach plot

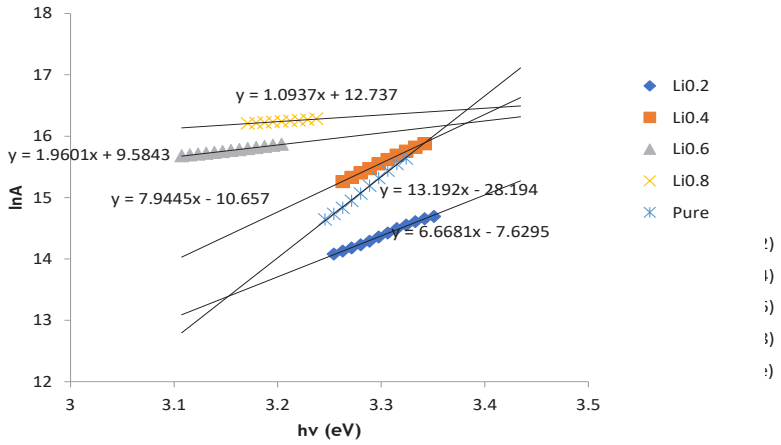

Fig. S10- lnA vs. hv for specimens prepared by sols with different ratio of Li/Zn.